INDIAN JOURNAL OF SCIENCE AND TECHNOLOGY

RESEARCH ARTICLE

Enhancing CIGS Solar Cell Performance with Erbium-Doped TiO_2 Nanomaterial: Simulation Study

J V Jayachithra[1]*, K Elampari[2], M Meena[3]

1 Research scholar, Department of Physics, S.T. Hindu College (affiliated to Manonmaniam Sundaranar University, Abishekapatti, Tirunelveli), Nagercoil, 629002, Tamilnadu, India
2 Associate Professor, Department of Physics, S.T. Hindu College, Nagercoil, 629002, Tamilnadu, India
3 Assistant Professor, Department of Physics, S.T. Hindu College, Nagercoil, 629002, Tamilnadu, India

OPEN ACCESS

Received: 01-08-2023
Accepted: 16-09-2023
Published: 25-10-2023

Citation: Jayachithra JV, Elampari K, Meena M (2023) Enhancing CIGS Solar Cell Performance with Erbium-Doped TiO_2 Nanomaterial: Simulation Study. Indian Journal of Science and Technology 16(40): 3453-3461. https://doi.org/10.17485/IJST/v16i40.1935

* **Corresponding author**.

jvjayachithra@gmail.com

Funding: None

Competing Interests: None

Published By Indian Society for Education and Environment (iSee)

ISSN
Print: 0974-6846
Electronic: 0974-5645

Abstract

Objectives: To find a proper rare earth-doped metal-oxide-based buffer layer for CIGS solar cells with improved performance that has less harmfulness than cadmium. **Methods:** This study concentrated on the synthesis of pure and Er-doped TiO_2 nanomaterials via microwave-assisted hydrothermal method and its characterization results. Additionally, to analyze the performance of TiO_2 and Er-doped TiO_2 as a buffer layer in a CIGS solar cell, numerical simulations were performed using the SCAPS-1D (Solar cell capacitance simulator) software. **Findings:** The positive outcomes came from the characterization results, which revealed that the synthesized nanomaterials have an anatase phase, microscopic crystallite size, and flower-like shape. The band gap effectively decreases from 3.45 eV for pure TiO_2 to 2.75 eV for Er-doped TiO_2, which effectively increases the absorption in the visible portion of the solar spectrum. The refractive indices of pure and Er-doped TiO_2 were calculated as 2.37 and 2.50 respectively from their corresponding band gaps. The results from the simulations showed that using a single buffer layer of Er-doped TiO_2 uplifted the performance of the CIGS solar cell, resulting in higher open circuit voltage, increased short-circuit current density with overall efficiency, η = 25.31% compared to pure TiO_2 and CdS-based dual buffer layers. **Novelty:** For the first time, the Er-TiO_2 nanomaterial was studied as buffer layer material. The numerical simulation and characterization findings justify the adoption of Er-TiO_2 as a buffer layer in CIGS solar cells.

Keywords: Hydrothermal method; Erbium; Buffer layer; CIGS; SCAPS

1 Introduction

The development of silicon (Si) solar cells opened the door for harnessing solar energy because they provide a sustainable and eco-friendly technique to produce electricity. Due to their high photovoltaic performance, cheap material cost, and versatility, CIGS

(copper indium gallium selenide) solar cells are a category of thin-film photovoltaic technology that has drawn considerable interest as a possible replacement for normal silicon-based solar cells.[1] The window layer, buffer layer, and absorber layer are the three main layers that makeup CIGS solar cells. Of these aforementioned layers, the researchers are more focused on the buffer layer. Since the buffer layer is crucial in helping the absorber layer by promoting the construction of the bridge that links the window layer and the absorber layer. Additionally, by adjusting the band alignment between the window and the absorber layer, the buffer layer can improve the charge carrier collection and lessen recombination-related losses.[2] Normally, Cadmium sulfide (CdS) has been extensively used as a buffer layer for CIGS due to its favorable band alignment with the absorber layer.[3] It is difficult to use CdS in real-world solar cell applications because of its harmful nature, which limits its use as a buffer layer in CIGS solar cells.[3]

Research investigations are concentrated on finding a better replacement for CdS. Several alternatives have been used to date like ZnO, ZnSe, ZnS, SiC, In_2S_3, $ZrS_xSe_{2-x,}$ and SnO_2.[4,5] The remarkable efficiency of 23.25% was noted by the researchers using $Zn[O,S,OH]_x/Zn_{0.8}Mg_{0.2}O$ as a dual buffer layer in the fabricated CIGSSe solar cell.[6] For this work, a less toxic metal oxide semiconductor material (namely titanium dioxide) was chosen as the buffer layer. TiO_2 is an appealing material for this application due to its wide band gap, flexible optical and electrical characteristics, chemical and thermal stability, and inexpensive, making it a promising option for large-scale solar cell production.[7] The simulation study of TiO_2 as a buffer layer in CIGS solar cells using AFORS-HET software gives an efficiency of 16.03%.[8] Reports suggest that adding rare-earth elements to TiO_2 can refine the band gap, increase carrier lifetime, and improve charge transport.[7] In this study, Erbium (Er), one of the rare earth materials, was used as a dopant, hoping to potentially enrich the performance of the TiO_2 buffer layer. The fabrication of dye-sensitized solar cells (DSSC) with Er-doped TiO_2 showed an efficiency of 4.62%, whereas DSSC with pure TiO_2 shows only 2.88%.[9] The TiO_2 and Er-doped TiO_2 nanomaterials were prepared via a single-step microwave-assisted hydrothermal process, offering advantages such as high yield, uniform size distribution, reduced reaction time, cost-effectiveness, and eco-friendliness.[10]

The present work covers the preparation of TiO_2 and Er-TiO_2 nanomaterials and the interpretation of characterization results obtained from powder X-ray diffraction (PXRD) analysis, high-resolution transmission electron microscopic (HR-TEM) analysis, and UV-visible spectroscopic analysis. Furthermore, the article discusses the numerical simulation of CIGS solar cells with TiO_2 and Er-TiO_2 as buffer layers using SCAPS-1D software.

2 Methodology

The precise steps involved in the preparation of the nanomaterials are schematized in Figure 1.

3 Results and Discussion

3.1 PXRD analysis

The 2θ and intensity values were recorded using a Rigaku Ultima IV X-Ray Diffractometer with a 1.5406 Å wavelength of CuKα radiation. The lattice parameters, the unit cell volume, (h k l) planes indexing, bravais lattice, and space group were identified using General Structure Analysis Software-II (GSAS-II).[11] The peaks of the pure and 1 mol% Er-doped TiO_2 nanomaterials belong to the anatase phase, which was known from the GSAS-II results, and it was also confirmed by correlating the peaks with JCPDS file no. 21-1272, which was schematized in Figure 2. Studies suggest that the efficient electron mobility of the anatase phase TiO_2 makes it a promising option to use in solar cells.[12]

The average crystallite size of the nanomaterials was calculated using the Debye-Scherrer relation.[9] The high-intensity peak of 1 mol% Er-doped TiO_2 was wider compared to the peak of pure TiO_2, leading to a decrease in crystallite size in Er-doped TiO_2 nanomaterials.[13] Venkatachalam et al. also reported the crystallite size reduction due to the wider peaks.[9] In addition, the parameters detailed in Table 1 show that the decrease in lattice parameters and the unit cell volume of the Er-doped TiO_2 may be significant due to the big ionic radius of the erbium ion (0.89 Å) whereas the ionic radius of titanium is 0.605 Å.[14] According to Table 1, the volume of the unit cell for Er-doped TiO_2 shrank along with the drop of the average crystallite size, possibly signifying that the entry of Er^{3+} ions led the surface area to rise by shrinking the unit cell, which is highly useful in photocatalytic behavior.[15] The capacity of the Er-TiO_2 nanomaterial to absorb light naturally increases with an increase in surface area.

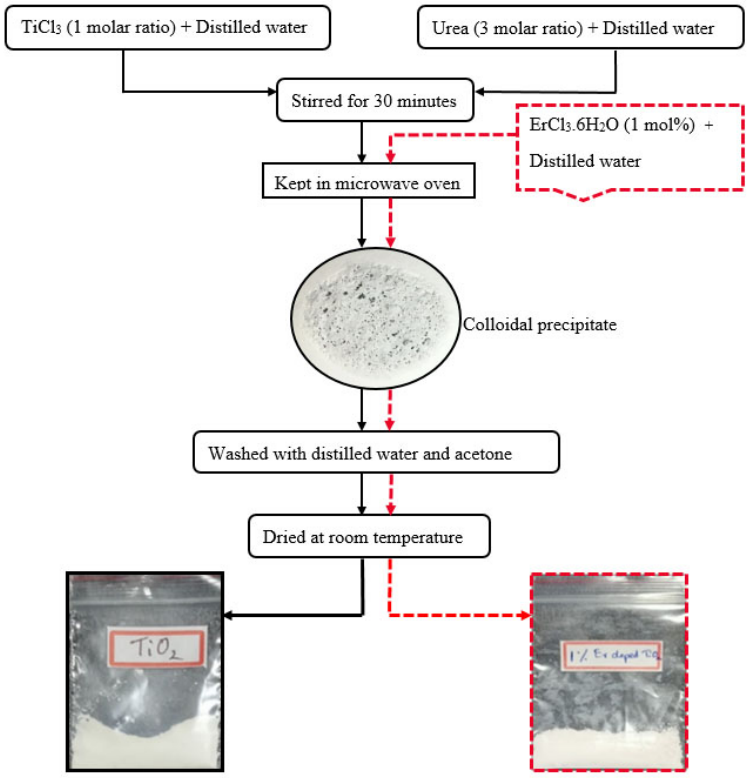

Fig 1. Synthesis procedure of pure and Er-doped TiO_2 nanomaterials

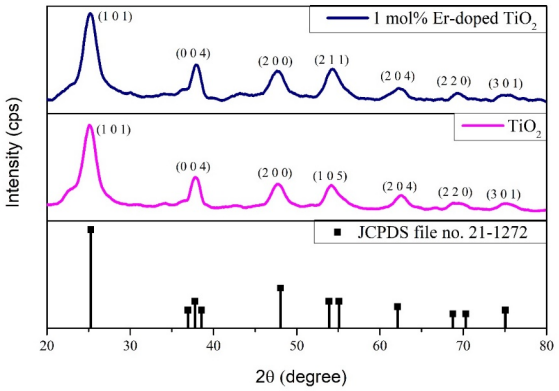

Fig 2. PXRD pattern of pure and Er-doped TiO_2 nanomaterials

Table 1. Parameters calculated using GSAS-II software

Nanomaterial	a=b (Å)	c (Å)	Volume of the unit cell ($Å^3$)	Structure	Space group	Average crystallite size, $D = \frac{k\lambda}{\beta Cos\theta}$ [nm]
TiO_2	3.82	9.50	138.27	tetragonal body-centered	$I4_1/amd$	5.41 [3]
1 mol% Er-doped TiO_2	3.82	9.45	137.68	tetragonal body-centered	$I4_1/amd$	5.19 [3]

3.2 HR-TEM analysis

The HR-TEM analysis was conducted using a JOEL TEM 2100 High-Resolution Transmission Electron Microscope. The TEM pictures of pure TiO_2 and 1 mol% Er-doped TiO_2 revealed a flower-like nanoparticle structure, as shown in Figure 3 [a] and [b]. The polycrystalline nature of the nanomaterials was visible through the rings observed in the Selected Area Electron Diffraction (SAED) pattern, which was seen in Figure 3 [c] and [d]. The d-spacing values were identified using ImageJ software.[16] The lattice fringe width (d-spacing) for the (101) plane was predicted as 3.65 Å and 3.571 Å, as portrayed in Figure 3 [e] and [f]. The (h k l) planes and d-spacing values discovered using ImageJ software were also validated by the GSAS-II results. Khursheed Ahmad et al. exposed that the nanomaterial with a flower-like structure has a large surface area when compared with other structures,[17] and hence, using a flower-structured material in solar cells may increase the cell's efficiency.

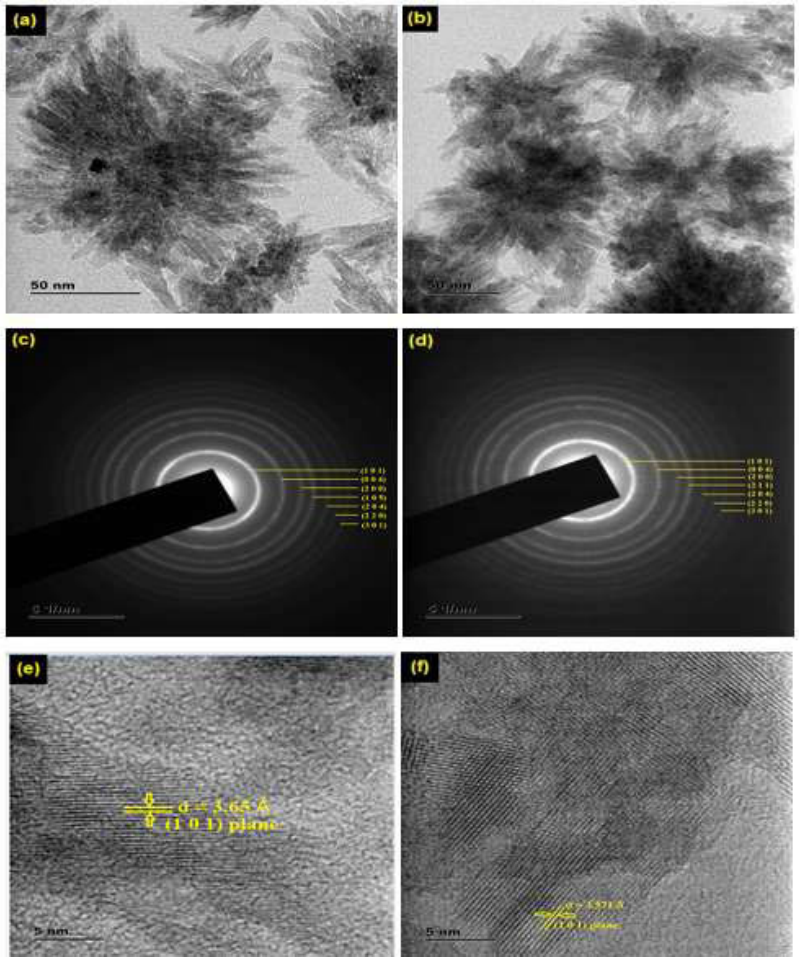

Fig 3. Comparison of TEM pictures, SAED pattern and lattice images of TiO_2 and Er-TiO_2

3.3 UV — visible spectroscopic analysis

The absorption characteristics of TiO_2 and Er-TiO_2 nanomaterials were examined using the JASCO UV-Vis spectrophotometer. The absorption spectra of TiO_2 nanomaterials exhibited peaks at 235 nm and 280 nm in the UV area, as revealed in Figure 4 [a]. In contrast, the absorption of 1 mol% Er-doped TiO_2 nanomaterials decreased in the UV region but increased in the visible region. The indirect band gap (Eg) of pure TiO_2 and 1 mol% Er-doped TiO_2 was determined to be 3.45 eV and 2.75 eV, respectively, using the Tauc plot (Figure 4 [b]). This kind of decrement in band gap value was also reported by Mutalib et al.[18] The considerable reduction in band gap may have been produced by oxygen vacancies brought on by the doping of Er^{3+} ions.[19]

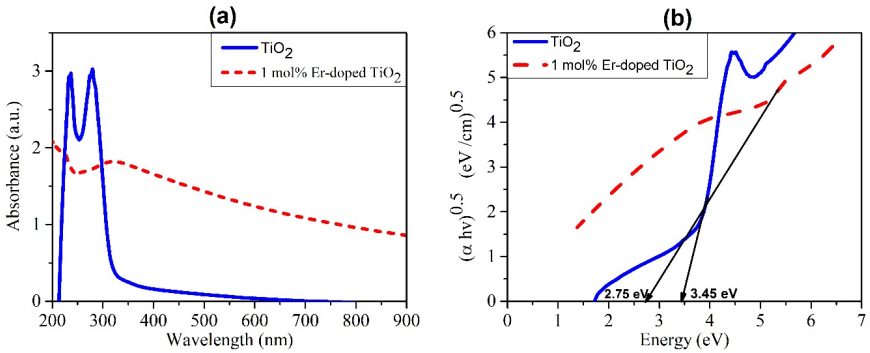

Fig 4. Images of [a] absorbance graph and [b] Tauc's plot

A CIGS solar cell's efficiency is closely correlated with the buffer layer's refractive index. Limiting reflection losses at the interface between the adjacent layers also depends on the buffer layer and the CIGS absorber layer's refractive index matching.[20] The increased reflection losses can be caused by an imbalance in the refractive indices, which decreases solar cell efficiency. The CIGS absorber layer's refractive index commonly falls between 2.54 and 3.05.[21] The refractive index (n) from the energy gap was calculated using Equation (1) presented by Ravindra et al.,[22]

$$E_g n^4 = 108 \tag{1}$$

The refractive index was calculated as 2.37 and 2.50 for TiO_2 and 1 mol% Er-doped TiO_2 respectively. These results indicate that due to the matching of the refractive index of Er-TiO_2 material with the absorbance layer, CIGS solar cells with an Er-doped TiO_2 buffer layer may have greater efficiency than CIGS solar cells based solely on TiO_2.

3.4 Modelling and simulation in SCAPS-1D

Numerical simulation has emerged as a cost-effective and time-efficient tool for studying solar cells and optimizing their designs. The SCAPS-1D is widely accepted for its accuracy and versatility in simulating solar cells.[4] The behavior of the cell in one direction typically perpendicular to the substrate can easily be studied in SCAPS-1D. The Equations (2), (3) and (4) which respectively describe Poisson's equation and continuity equations, both explain how charges move through the device.[5]

$$\frac{\partial^2 \varnothing}{\partial x^2} = -\frac{q}{\varepsilon}\left[p - n + N_D^+ - N_A^- + \frac{\rho_{def}}{q}\right] \tag{2}$$

$$-\frac{\partial J_n}{\partial x} - R_n + G[x] = \frac{\partial n}{\partial t} \tag{3}$$

$$-\frac{\partial J_p}{\partial x} - R_p + G[x] = \frac{\partial p}{\partial t} \tag{4}$$

Where ϕ - electrostatic potential [V], ε - dielectric constant of the material, q - electric charge [C], p - hole concentration [m^{-3}], n - electron concentration [m^{-3}], N_D^+ - donor concentration [cm^{-3}], N_A^- - acceptor concentration [cm^{-3}], ρ_{def} - defect charge density [cm^{-3}], J_n - electron current density [A/m^2], J_p - hole current density [A/m^2], R_n - electron recombination rate [cm^{-3}] and R_p - hole recombination rate [cm^{-3}].

The electron-hole pair generated during the simulation was given as the generation (G[x]) as in the Equation (5).

$$G(x) = \int_{\lambda_{min}}^{\lambda_{max}} \alpha(\lambda, x) \; . \; N_{photon}(\lambda, x) d\lambda \tag{5}$$

Where λ_{min} - minimum wavelength [m] and λ_{max} - maximum wavelength [m], α – absorption coefficient [1/m], and N_{photon} - spectrum of the incident photon.

3.4.1 Device configuration and simulation of the proposed CIGS solar cell

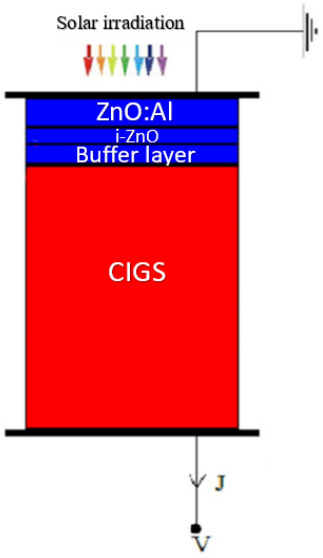

Fig 5. SCAPS simulated CIGS solar cell device structure

The simulated CIGS solar cell has the succeeding structure: front contact/ZnO:Al/i-ZnO/buffer layer/CIGS/back contact as shown in Figure 5. The in-built solar spectrum file AM1.5G of the SCAPS 1-D was used in the simulation. Specifically, the cell's temperature was fixed at 300 K. The work done by Mebelson et al. served as the basis for the ZnO:Al, CdS, and CIGS layer specifications.[(1)] The layer parameters of i-ZnO used here were loaded from SCAPS. Except for the bandgap and dielectric permittivity, the other parameters of TiO_2 and Er-TiO_2 were all set to default, which are listed in Table 2. A 60 nm thick buffer layer was utilized in this simulation. The simulation employed five distinct buffer layer configurations, including single buffer layers of TiO_2 and Er-TiO_2, and dual buffer layers consisting of TiO_2/CdS, Er-TiO_2/CdS, and TiO_2/Er-TiO_2.

Table 2. List of parameters used in the simulation

Parameters	ZnO:Al	i-ZnO	CdS	TiO_2	Er-TiO_2	CIGS
Thickness [nm]	200	55	variable	variable	variable	2000
Bandgap [eV]	3.3	3.400	2.400	3.45	2.75	1.2
Electron affinity [eV]	4.4	4.000	4.200	3.9	3.9	3.89
Dielectric permittivity [relative]	10	9.000	10.000	17.80	13.78	13.6
CB effective density of states [1/cm^3]	2.2E+18	2.2E+18	2.2E+18	1.0E+19	1.0E+19	2.2E+18
VB effective density of states [1/cm^3]	1.8E+19	1.8E+19	1.8E+19	1.0E+19	1.0E+19	1.8E+19
Electron thermal velocity [cm/s]	1.0E+7	1.0E+7	1.0E+7	1.0E+7	1.0E+7	1.0E+7
Hole thermal velocity [cm/s]	1.0E+7	1.0E+7	1.0E+7	1.0E+7	1.0E+7	1.0E+7
Electron mobility [cm^2/Vs]	10.0E+1	5.000E+1	5.000E+0	2.0E+1	2.0E+1	2.5E+1
Hole mobility [cm^2/Vs]	2.5E+1	5.000E+0	5.000E+0	1.0E+1	1.0E+1	1.0E+1
Shallow uniform donor density ND [1/cm^3]	5.000E+17	5.000E+17	1.000E+18	1.0E+16	1.0E+16	-
Shallow uniform acceptor density NA [1/cm^3]	-	-	-	-	-	5.000E+17

3.4.2 Analysis of current density-voltage curve

The J-V graph can expose significant parameters such as the fill factor (FF), short-circuit current density (J_{SC}), and open-circuit voltage (V_{OC}). These variables offer insightful data regarding the functionality and effectiveness of the solar cell. The FF and efficiency (η) were calculated by using the Equations (6) and (7).[23]

$$FF = \frac{V_{max} \times I_{max}}{V_{oc} \times I_{sc}} \tag{6}$$

$$\eta = \frac{V_{oc} \times I_{sc} \times FF}{Intensity\ of\ light} \times 100\% \tag{7}$$

The J-V curve for the single-layer Er-TiO_2 solar cell shown in Figure 6 [a] performs particularly well among the simulated CIGS solar cells. The inset graph in Figure 6 [a] shows an enlarged view of the variation of current density in different buffer layers. The V_{oc} values for the various buffer layers are relatively similar, differing from 0.7312 V to 0.7319 V. The Jsc values for the different buffer layers are also quite alike, ranging from 40.16 mA/cm^2 to 41.02 mA/cm^2. All five chosen buffer layers exhibited nearly identical maximum voltage and current output when irradiated with the AM1.5G spectrum. However, there was noticeable variability in the FF and η values across the different buffer layers. The Er-TiO_2 and TiO_2/Er-TiO_2 buffer layers have the highest FF value of 84.30 %, while the TiO_2/CdS buffer layer has the lowest FF value of 84.05 %.

Findings in Table 3 demonstrate that the efficiency of CIGS solar cells with TiO_2-based buffer layers (TiO_2, Er-TiO_2, and TiO_2/Er-TiO_2) are on par with or superior to those with CdS-based buffer layers (TiO_2/CdS and Er-TiO_2/CdS). Particularly, compared to the CdS-based buffer layers, the TiO_2-based buffer layers exhibit a marginally greater efficiency. The efficiencies of the TiO_2/CdS and Er-TiO_2/CdS buffer layers are 24.86% and 25.15%, respectively, while those of the TiO_2, Er-TiO_2, and TiO_2/Er-TiO_2 buffer layers are 24.75%, 25.31%, and 25.04%. The simulation work done by Leila Ghalmi et al. reported an efficiency of 23.12% for CIGS solar cells with a ZnS-buffer layer.[24] Thus, the current investigation shows that TiO_2-based buffer layers for CIGS solar cells are an effective substitute for CdS-based buffer layers since they can deliver comparable or higher performance.

Table 3. Output parameters obtained from the simulation

Buffer layer materials	V_{oc} [V]	J_{sc} [mA/cm^2]	FF [%]	η [%]
TiO_2	0.7312	40.16	84.27	24.75
Er-TiO_2	0.7319	41.02	84.30	25.31
TiO_2/CdS	0.7313	40.44	84.05	24.86
Er-TiO_2/CdS	0.7316	40.89	84.07	25.15
TiO_2/Er-TiO_2	0.7316	40.59	84.30	25.04

3.4.3 Analysis of quantum efficiency (QE) curve

The Quantum efficiency of a solar cell is proportional to the number of charge carriers produced in the external circuit by incident photons of a particular wavelength. The quantum efficiency graph of the CIGS solar cells with Er-TiO_2, TiO_2/CdS, Er-TiO_2/CdS, and TiO_2/Er-TiO_2 as the buffer layers were almost looking similar, which was visible in Figure 6 [c] and [d]. On the other hand, the CIGS solar cell's quantum efficiency, which is based on TiO_2 begins at a wavelength of 700 nm as shown in Figure 6 [b].

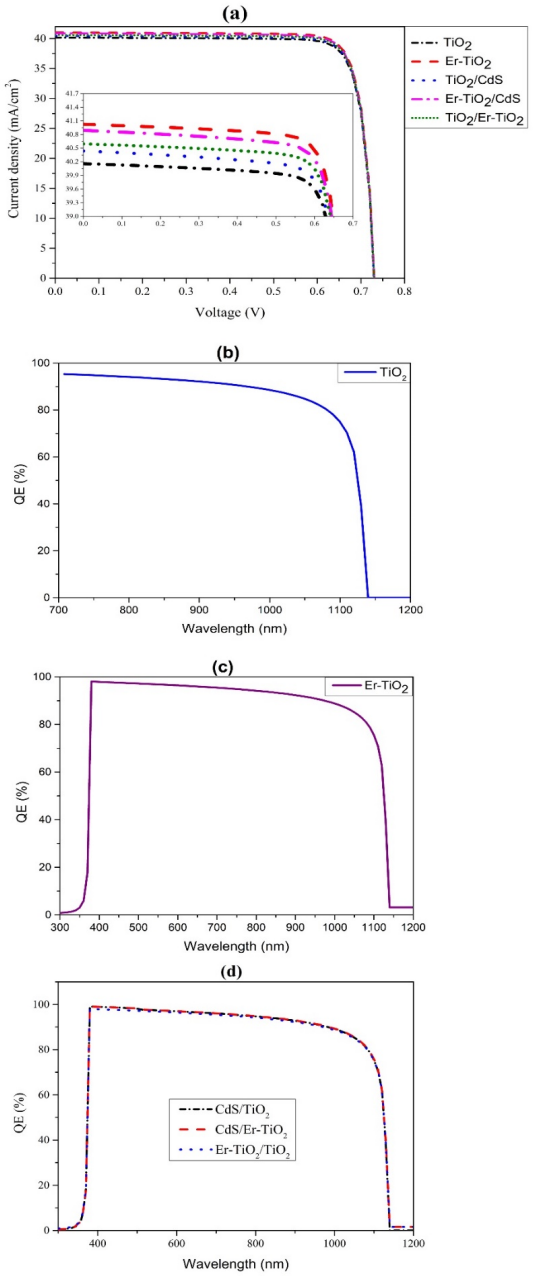

Fig 6. J-V curve and QE curve of the simulated CIGS solar cell

4 Conclusion

Using a single stage of microwave assistance, hydrothermal preparation was used to synthesize anatase TiO_2 and Er-doped TiO_2 nanomaterials. After the addition of Er^{3+} ions to TiO_2, favorable results were obtained, like a small crystallite size and a reduction of the band gap. For the very first time, the CIGS solar cells with TiO_2, Er-TiO_2, TiO_2/CdS, Er-TiO_2/CdS, and TiO_2/Er-TiO_2 as buffer layers were simulated and their J-V characteristic curves were analyzed. TiO_2 shows an efficiency of 24.75%, but its quantum efficiency is poor. Er-doped TiO_2 with 25.31% efficiency (percentage of increase is 2.26%) shows a good spectral response as a CdS-based dual buffer layer. In addition, there is no significant difference between the efficiencies of the Er-TiO_2-based and CdS-based CIGS solar cells. Besides, TiO_2-based nanomaterials are less toxic and more environmentally

friendly than CdS, which is an additional advantage for their use in solar cell applications. These results recommend that erbium-doped TiO_2 can be a hopeful candidate to serve as a buffer layer in CIGS solar cells.

5 Acknowledgement

The authors are thankful to the Physics Research Centre, S.T. Hindu College, Nagercoil, for providing the facilities to carry out this research work. Also, the authors are thankful to Dr. Marc Burgelman, University of Gent, Belgium, for providing the SCAPS-1D simulation software.

References

1) Mebelson TJ, Elampari K. Numerical simulation for optimal thickness combination of CdS/ZnS dual buffer layer CuInGaSe2 solar cell using SCAPS 1D. *Indian Journal of Science and Technology*. 2019;12(45):1–6. Available from: https://doi.org/10.17485/ijst/2019/v12i45/148395.
2) Sinha S, Nandi DK, Pawar PS, Kim SH, Heo J. A review on atomic layer deposited buffer layers for Cu(In,Ga)Se2 (CIGS) thin film solar cells: Past, present, and future. *Solar Energy*. 2020;209:515–537. Available from: https://doi.org/10.1016/j.solener.2020.09.022.
3) Sobayel MK, Chowdhury MS, Hossain T, Alkhammash HI, Islam S, Shahiduzzaman M, et al. Efficiency enhancement of CIGS solar cell by cubic silicon carbide as prospective buffer layer. *Solar Energy*. 2021;224:271–278. Available from: https://doi.org/10.1016/j.solener.2021.05.093.
4) Rahman MA. Enhancing the photovoltaic performance of Cd-free Cu2ZnSnS4 heterojunction solar cells using SnS HTL and TiO2 ETL. *Solar Energy*. 2021;215:64–76. Available from: https://doi.org/10.1016/j.solener.2020.12.020.
5) Moustafa M, Zoubi TA, Yasin S. Optoelectronics Simulation of CIGS-Based Solar Cells Using a Cd-Free Nontoxic ZrSxSe2−x as a Novel Buffer Layer. *Brazilian Journal of Physics*. 2022;52(4):1–10. Available from: https://doi.org/10.1007/s13538-022-01146-z.
6) Park H, Alhammadi S, Reddy VRM, Park C, Kim WK. Influence of the Al-Doped ZnO Sputter-Deposition Temperature on Cu(In,Ga)Se2 Solar Cell Performance. *Nanomaterials*. 2022;12(19):1–18. Available from: https://doi.org/10.3390/nano12193326.
7) Borrego-Pérez JA, González F, Meza-Avendaño CA, Santos IMDL, López-Juárez RM, Hernández I, et al. Structural, optical and photoluminescence properties of TiO2 and TiO2: Tm3+ nanopowders. *Optik*. 2021;227:166083. Available from: https://doi.org/10.1016/j.ijleo.2020.166083.
8) Gagandeep, Singh M, Kumar R, Kumari S. Numerical simulation of n-TiO2/p-CIGS solar cell. In: Dae Solid State Physics Symposium 2019;vol. 2265, Issue 1 of AIP Conference Proceedings. AIP Publishing. 2020. Available from: https://doi.org/10.1063/5.0017203.
9) Venkatachalam P, Kalaivani T, Krishnakumar N. Erbium doped anatase TiO2 nanoparticles for photovoltaic applications. *Optical and Quantum Electronics*. 2019;51(9):1–16. Available from: https://doi.org/10.1007/s11082-019-2034-2.
10) Omo-Okoro PN, Maepa CE, Daso AP, Okonkwo JO. Microwave-Assisted Synthesis and Characterization of an Agriculturally Derived Silver Nanocomposite and Its Derivatives. *Waste and Biomass Valorization*. 2020;11(5):2247–2259. Available from: https://doi.org/10.1007/s12649-018-0523-3.
11) Altin S, Korkusuz K. Fabrication, electrochemical performance, and in situ infrared thermal imaging of Na0.67[Mn0.5Fe0.5]1-xCuxO2 battery cells. *International Journal of Energy Research*. 2021;45(9):13809–13821. Available from: https://doi.org/10.1002/er.6711.
12) Nowsherwan GA, Zaib A, Shah AA, Khan M, Shakoor A, Bukhari SNS, et al. Preparation and Numerical Optimization of TiO2:CdS Thin Films in Double Perovskite Solar Cell. *Energies*. 2023;16(2):1–22. Available from: https://doi.org/10.3390/en16020900.
13) Sivakumar S, Robinson Y, Mala NA. Studies on photocatalytic performance and supercapacitor applications of undoped and Cu-doped ZnO nanoparticles. *Applied Surface Science Advances*. 2022;12:1–14. Available from: https://doi.org/10.1016/j.apsadv.2022.100344.
14) Sayed OE, Battisha I, Lahmar A, Marssi ME. Er3+ and Er3+/Yb3+ ions embedded in nano-structure BaTi0.9Sn0.1O3: structure, morphology and dielectric properties. *World Journal of Nano Science and Engineering*. 2021;11(2):25–43. Available from: https://www.scirp.org/journal/paperinformation.aspx?paperid=111149.
15) Barkat F, Afzal M, Khan BS, Saeed A, Bashir M, Mukhtar A, et al. Formation Mechanism and Lattice Parameter Investigation for Copper-Substituted Cobalt Ferrites from Zingiber officinale and Elettaria cardamom Seed Extracts Using Biogenic Route. *Materials*. 2022;15(13):1–19. Available from: https://doi.org/10.3390/ma15134374.
16) Khan SA, Patel S, Shukla P, Kumar R, Dixit R. Synthesis and Characterization of PVP embedded Silver Nanoparticles to Study their Structural and Optical Properties. *Journal of Scientific Research*. 2022;66(04):139–143. Available from: https://www.bhu.ac.in/research_pub/jsr/Volumes/JSR_66_04_2022/20.pdf.
17) Ahmad K, Mobin SM. High surface area 3D-MgO flowers as the modifier for the working electrode for efficient detection of 4-chlorophenol. *Nanoscale Advances*. 2019;1(2):719–727. Available from: DOIhttps://doi.org/10.1039/C8NA00007G.
18) Mutalib MA, Ludin NA, Su'ait MS, Davies M, Sepeai S, Teridi MAM, et al. Performance-Enhancing Sulfur-Doped TiO2 Photoanodes for Perovskite Solar Cells. *Applied Sciences*. 2022;12(1):1–10. Available from: https://doi.org/10.3390/app12010429.
19) Prakash J, Samriti, Kumar A, Dai H, Janegitz BC, Krishnan V, et al. Novel rare earth metal–doped one-dimensional TiO2 nanostructures: Fundamentals and multifunctional applications. *Materials Today Sustainability*. 2021;13:100066. Available from: https://doi.org/10.1016/j.mtsust.2021.100066.
20) Rafieipour P, Mohandes A, Moaddeli M, Kanani M. Integrating transfer matrix method into SCAPS-1D for addressing optical losses and per-layer optical properties in perovskite/Silicon tandem solar cells. 2023. Available from: https://doi.org/10.48550/arXiv.2308.01132.
21) Baik J, Park J, Lee G, Kim S, Kim J. Effects of Incoherent Front Cover Glass on Current-Voltage Characteristics of Cu(In,Ga)Se2 Solar Cells: Investigation into Calculation Accuracy for Cover Glass Modeled as Optically Coherent or Incoherent. *Applied Sciences*. 2020;10(9):1–16. Available from: https://doi.org/10.3390/app10093312.
22) Chandrashekaraiah G, Reddy CN, Gowda VCV, Mallikarjunaiah KJ. UV-Vis absorption spectroscopic analysis of Er3+ ion doped oxyhalide glasses. *Materials Today: Proceedings*. 2022;49(Part 5):1646–1649. Available from: https://doi.org/10.1016/j.matpr.2021.07.426.
23) Bodur MC, Duman S, Orak I, Saritas S, Baris O. The photovoltaic and photodiode properties of Au/Carmine/n-Si/Ag diode. *Optics & Laser Technology*. 2023;162:109251. Available from: https://doi.org/10.1016/j.optlastec.2023.109251.
24) Ghalmi L, Bensmaine S, Merzouk CEH. Numerical Simulation Study of CIGS-based Thin Film and Heterojunction Solar Cells: Doping and Buffer/Absorber Layer Optimization for Maximum Efficiency. *Journal of Renewable Energies*. 2023;1(ICARES 2022 (Special Issue)):51–63. Available from: https://doi.org/10.54966/jreen.v1i1.1098.